

Dynamic transition and resonance in current-driven arrays of Josephson junctions

Gun Sang Jeon

*Center for Strongly Correlated Materials Research,
Seoul National University, Seoul 151-747, Korea*

Jong Soo Lim, Hyun Jin Kim, and M.Y. Choi

Department of Physics, Seoul National University, Seoul 151-747, Korea

We consider a two-dimensional fully frustrated Josephson-junction array, which is driven uniformly by oscillating currents. As the temperature is lowered, there emerges a dynamic phase transition to an ordered state with nonzero dynamic order parameter for small currents. The transition temperature decreases monotonically with the driving amplitude, approaching zero at a certain critical value of the amplitude. Above the critical value, the disordered phase and the dynamically ordered phase are observed to appear alternatively. The characteristic stochastic resonance behavior of the system is also examined, which reveals that the resonance behavior of odd and even harmonics can be different according to the zero-temperature state.

PACS numbers: 74.50.+r, 74.25.Nf, 05.40.-a

I. INTRODUCTION

Dynamic responses of cooperatively interacting many-body systems to time driven perturbations are extremely important technologically and involve intriguing physics, resulting in intensive investigation in recent years. Among the well-known systems is the simple kinetic Ising model under oscillating magnetic fields.^{1,2,3} It has been revealed that spontaneous symmetry breaking takes place at a finite strength of the oscillating field^{1,2} and that in two dimensions the transition belongs to the same universality class as the equilibrium two-dimensional (2D) Ising model.² The stochastic resonance (SR) phenomena have also been studied.³

Another interesting example is the dynamics of the fully frustrated Josephson-junction array (FFJJA), which possesses the same Z_2 symmetry as the Ising model in addition to the continuous $U(1)$ symmetry. Unlike the Ising model, the FFJJA has real intrinsic dynamics derived from the Josephson relations and thus grants direct experimental realizations. There have been some studies on the dynamic properties of the FFJJA^{4,5} and recently dynamic transitions have also been investigated in the FFJJA driven by uniform dc currents⁶ or staggered oscillating magnetic fields.⁷ Similarly to the kinetic Ising model, the FFJJA driven by staggered oscillating fields has been shown to exhibit a dynamic phase transition and an SR behavior. In the presence of weak fields, the dynamic phase transition belongs to the same universality class as the equilibrium Z_2 transition in the fully frustrated XY (FFXY) model. At strong fields, in contrast, a different universality class has been suggested.

In this paper, we investigate the FFJJA in the presence of uniform oscillating currents, which is easier to realize in experiment than the system under staggered oscillating magnetic fields. The dynamic properties of the system is examined with attention paid to the dynamic transition and the SR phenomena. At low tem-

peratures the chirality in the FFJJA displays antiferromagnetic ordering. To describe the dynamic transition associated with the antiferromagnetic ordering of the chirality, we introduce the dynamic order parameter, which is the staggered magnetization averaged over one period of the uniform oscillating current, and investigate its behavior with respect to the amplitude and the frequency of the driving current as well as to the temperature. At zero temperature, as the driving amplitude is raised, the dynamically ordered phase and the disordered one are observed to appear alternatively. As the temperature is increased, the ordered phase undergoes a dynamic phase transition to the disordered phase. Through the use of the finite-size scaling analysis, the dynamic transition is shown to belong to the same universality class as the equilibrium Z_2 transition present in the FFX Y . We also examine the SR phenomena in the system. As manifested by the signal-to-noise ratio (SNR) at several harmonics, odd and even harmonics are revealed to exhibit different SR behaviors. It is discussed in view of the variation of the zero-temperature states with the driving current amplitude.

This paper consists of five sections: Section II introduces the fully frustrated Josephson-junction array, driven uniformly by alternating currents, together with the dynamic order parameter, describing the dynamic transition of the system, and presents the zero-temperature behavior. In Sec. III the behavior of the dynamic order parameter at finite temperatures is investigated in detail, on the basis of which the dynamic phase diagram is constructed on the plane of the temperature and the driving amplitude. The nature of the transition is also examined and the equilibrium Z_2 universality class is identified. Section IV is devoted to the power spectrum of the staggered magnetization and the corresponding signal-to-noise ratio, which reveals the characteristic resonance behavior of the system with the appropriate values of the parameters. Finally, a brief summary is given in Sec. V.

II. FULLY FRUSTRATED ARRAY DRIVEN BY ALTERNATING CURRENT

To begin with, we consider the equations of motion for phase angles $\{\phi_i\}$ of the superconducting order parameters in grains forming an $L \times L$ square lattice with unit lattice constant. Within the resistively-shunted-junction model under the fluctuating twist boundary conditions,⁸ they read:

$$\sum_j' \left[\frac{d\tilde{\phi}_{ij}}{dt} + \sin(\tilde{\phi}_{ij} - \mathbf{r}_{ij} \cdot \Delta) + \eta_{ij} \right] = 0, \quad (1)$$

where the primed summation runs over the nearest neighbors of grain i and the thermal noise current η_{ij} satisfies $\langle \eta_{ij}(t)\eta_{kl}(t') \rangle = 2T\delta(t-t')(\delta_{ik}\delta_{jl} - \delta_{il}\delta_{jk})$ at temperature T . We have used the abbreviation $\tilde{\phi}_{ij} \equiv \phi_i - \phi_j - A_{ij}$ and $\mathbf{r}_{ij} \equiv \mathbf{r}_i - \mathbf{r}_j$ with $\mathbf{r}_i = (x_i, y_i)$ denoting the position of grain i . Note that \mathbf{r}_{ij} for nearest neighboring grains is a unit vector since the lattice constant has been set equal to unity. We have also written the energy and the time in units of $\hbar i_c/2e$ and $\hbar/2eRi_c$, respectively, with the critical current i_c and the shunt resistance R . The dynamics of the twist variables $\Delta \equiv (\Delta_x, \Delta_y)$, which are included in the fluctuating twist boundary conditions to allow fluctuations in the phase difference across the whole system, is governed by the equations

$$\begin{aligned} \frac{d\Delta_x}{dt} &= \frac{1}{L^2} \sum_{\langle ij \rangle_x} \sin(\tilde{\phi}_{ij} - \Delta_x) + \eta_{\Delta_x} - I_0 \sin(\Omega t), \\ \frac{d\Delta_y}{dt} &= \frac{1}{L^2} \sum_{\langle ij \rangle_y} \sin(\tilde{\phi}_{ij} - \Delta_y) + \eta_{\Delta_y}, \end{aligned} \quad (2)$$

where $\sum_{\langle ij \rangle_a}$ denotes the summation over all nearest neighboring pairs in the $a (= x, y)$ direction, η_{Δ_a} satisfies $\langle \eta_{\Delta_a}(t + \tau)\eta_{\Delta_{a'}}(t) \rangle = (2T/L^2)\delta(\tau)\delta_{a,a'}$, and the oscillating current $I_0 \sin(\Omega t)$ is injected in the x direction. In the Landau gauge, the bond angle A_{ij} , given by the line integral of the vector potential, takes the values

$$A_{ij} = \begin{cases} 0 & \text{for } \mathbf{r}_j = \mathbf{r}_i + \hat{\mathbf{x}} \\ \pi x_i & \text{for } \mathbf{r}_j = \mathbf{r}_i + \hat{\mathbf{y}} \end{cases}.$$

For the study of the transition associated with the Z_2 symmetry in the FFJJA, it is convenient to consider the chirality

$$C(\mathbf{R}, t) \equiv \text{sgn} \left[\sum_{\mathbf{P}} \sin(\tilde{\phi}_{ij}(t) - \mathbf{r}_{ij} \cdot \Delta(t)) \right] \quad (3)$$

and the staggered magnetization

$$m(t) \equiv \frac{1}{L^2} \sum_{\mathbf{R}} (-1)^{x_i + y_i} C(\mathbf{R}, t), \quad (4)$$

where $\sum_{\mathbf{P}}$ denotes the directional plaquette summation of links around the dual lattice site $\mathbf{R} \equiv \mathbf{r}_i + (1/2)(\hat{\mathbf{x}} + \hat{\mathbf{y}})$.

To probe the dynamic transition in the presence of an oscillating uniform current, we define the dynamic order parameter as the staggered magnetization averaged over one period of the oscillating current

$$Q \equiv \frac{\Omega}{2\pi} \left| \oint m(t) dt \right|. \quad (5)$$

In the numerical calculation, the sets of the equations of motion in Eqs. (1) and (2) are integrated via the modified Euler method with time steps of size $\Delta t = 0.05$. We have varied the step size, only to find no essential difference. Typically, data have been averaged over 5000 driving periods after the data obtained from the initial 1000 periods discarded; the appropriate stationarity has been verified. In addition, five independent runs have been performed, over which the average has also been taken, and systems of size up to $L = 32$ have been considered.

In the FFJJA, it is well known that there are two kinds of antiferromagnetic chirality ordering at zero temperature. The injection of uniform oscillating currents plays the role of tilting sinusoidally the 2D ‘‘egg-carton’’ lattice pinning potential. Accordingly, if the driving amplitude I_0 of the injected currents is large enough to overcome the lattice pinning potential, oscillations between the two ground states are expected to take place. In Fig. 1, we display the time evolution of the staggered magnetization $m(t)$ at zero temperature, evolved from the initial condition $m(t=0) = 1$ for driving frequency $\Omega/2\pi = 0.08$. For small I_0 , the system is shown to stay in the state with $m(t) = 1$ in spite of the driving current. When the amplitude exceeds the value $I_0^{(0)} \approx 1.01$, the system is driven out of the $m = 1$ state and the staggered magnetization oscillates between $m = \pm 1$; this arises since the chirality lattice moves collectively over the lattice potential under large current driving. In case that the driving induces the chirality lattice to move over only a single lattice barrier in the first half of the period, the system oscillates between the two ground states symmetrically (see the staggered magnetization for $I_0 = 1.50$ in Fig. 1). On the other hand, further increase of I_0 allows the chirality lattice to go over another barrier and yields asymmetric oscillations of the system between the ground states, as demonstrated by the staggered magnetization for $I_0 = 2.0$ in Fig. 1. The symmetry is restored and broken alternatively with the increase of I_0 , which is manifested by the zero-temperature behavior of Q with I_0 in Fig. 2. As expected in Fig. 1, the dynamic order parameter Q , which is unity below $I_0^{(0)}$, is shown to decrease abruptly to zero for $I > I_0^{(0)}$. Further increase of I_0 reveals that the dynamically ordered state ($Q > 0$) and the disordered one ($Q = 0$) appear alternatively in the system. It is observed that the saturation value of Q is less than unity and that the peak value of Q in each ordered region decreases monotonically with I_0 . Note also that the increase of the driving frequency Ω enhances the value of $I_0^{(0)}$ and moves the dynamically ordered regions

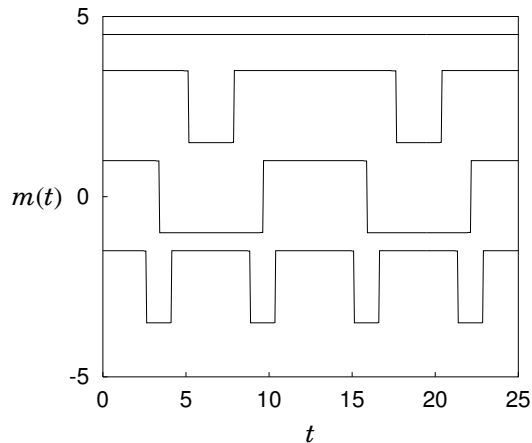


FIG. 1: Time evolution of the staggered magnetization at zero temperature for driving frequency $\Omega/2\pi = 0.08$ and amplitudes $I_0 = 0.98, 1.03, 1.50,$ and 2.0 from above. For clarity, the data for $I_0 = 0.98$ and 1.03 have been shifted upward by 3.5 and 2.5 , respectively, whereas those for $I_0 = 2.0$ shifted downward by 2.5 .

to larger values of I_0 , which reflects that a higher frequency implies a shorter period and accordingly, larger driving is necessary to move the chirality lattice over the lattice barrier within the (shorter) period. Except for the scale, however, the overall behavior at zero temperature does not change qualitatively with Ω .

III. DYNAMIC TRANSITION

We next investigate the effects of the temperature. At sufficiently high temperatures, thermal fluctuations are dominant so that the influence of the driving current and the lattice pinning potential can be neglected. Consequently, at high temperature, the staggered magnetization should fluctuate randomly with time, resulting in the vanishing dynamic order parameter. On the other hand, at low temperatures, where thermal fluctuations are small, the system is expected to be driven mainly by the oscillating uniform currents, exhibiting behavior similar to that at zero temperature. Accordingly, we expect a phase transition between the dynamically ordered phase and the disordered one as the temperature is varied. Figure 3, in which the ensemble average of the dynamic order parameter $\langle Q \rangle$ is plotted as a function of the temperature T for various driving amplitudes, explicitly shows the existence of such a transition between the dynamically ordered phase and the disordered one. The dynamic order parameter, starting from zero at high temperatures, develops as the temperature is lowered. It then grows rapidly and saturates eventually to the zero-temperature value as the temperature approaches zero. In particular, for I_0 above $I_0^{(0)}$, Fig. 3(b) shows that the zero-temperature value of $\langle Q \rangle$ is reduced rapidly with the

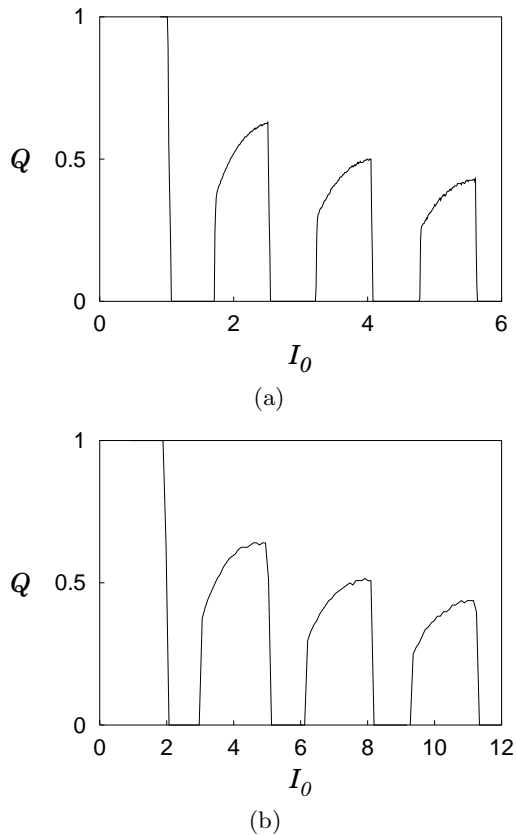


FIG. 2: Dynamic order parameter as a function of the driving amplitude at zero temperature in the system of size $L = 16$ with (a) $\Omega/2\pi = 0.08$; (b) $\Omega/2\pi = 0.16$.

increase of I_0 . Here, it is interesting that the apparent peak of $\langle Q \rangle$ is observed at a certain finite temperature rather than at zero temperature.

To estimate the transition temperature, we consider Binder's cumulants⁹

$$U_L = 1 - \frac{\langle Q^4 \rangle}{3\langle Q^2 \rangle^2}. \quad (6)$$

Since this quantity is size-independent at the transition temperature, the transition temperature can be determined from the crossing point of U_L for several sizes L . In Fig. 4, we plot the resulting phase diagram on the $T-I_0$ plane, displaying dynamic phase boundaries. The transition temperature initially decreases monotonically to zero as the driving amplitude I_0 is increased. However, further increase of I_0 drives the system into another ordered region, where the transition temperature first grows with the driving current, then reduces to zero. The zero-temperature results shown in Fig. 2 suggest that these additional ordered regions emerge repeatedly with the amplitude I_0 raised although the peak values of the transition temperature in these regions should decrease with I_0 . As the driving frequency Ω is increased, on the other hand, the transition temperature also increases

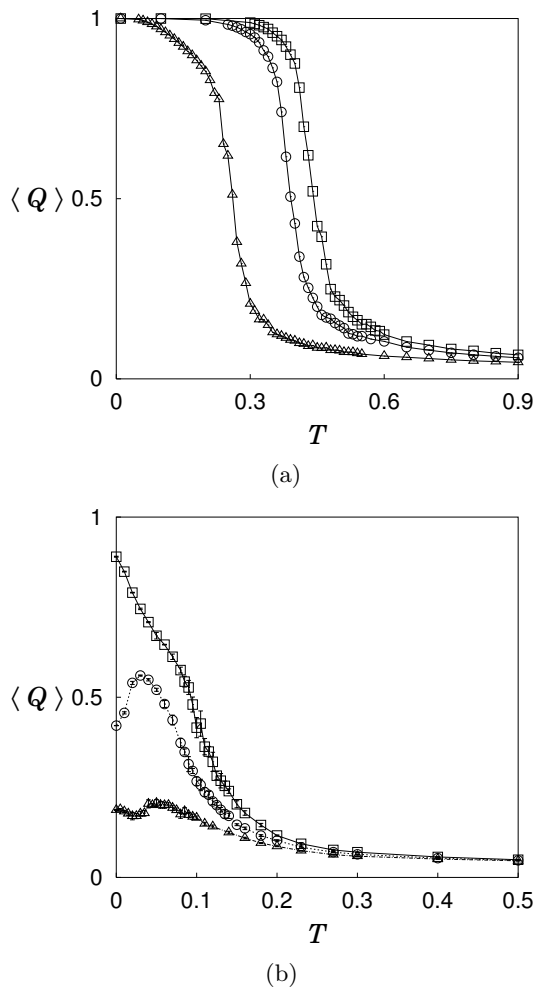


FIG. 3: Dynamic order parameter as a function of the temperature in the system of size $L = 16$ for various driving amplitudes (a) $I_0 = 0.3(\square), 0.5(\circ), 0.8(\triangle)$; (b) $I_0 = 1.02(\square), 1.04(\circ), 1.06(\triangle)$. Error bars have been estimated from standard deviations; in (a) they are not larger than the sizes of the symbols. Lines are merely guides to eyes.

and the dynamically ordered region expands on the $T-I_0$ plane. It is thus concluded that high driving frequency helps to maintain the dynamic order, which is consistent with the zero-temperature result in Fig. 2. It should also be noted here that cooling and heating curves for the dynamic order parameter do not exhibit any appreciable hysteresis even in the strong-current regime.

To probe the nature of the transition, we consider the scaling relation for the dynamic order parameter

$$\langle Q \rangle = L^{-\beta/\nu} f\left((T - T_c)L^{1/\nu}\right) \quad (7)$$

and plot $\langle Q \rangle L^{\beta/\nu}$ versus $(T - T_c)L^{1/\nu}$ for various sizes. Figure 5 exhibits the resulting scaling plots for the driving amplitude (a) $I_0 = 0.3$ and (b) $I_0 = 2.2$, with the critical exponents: (a) $\nu = 0.82$ and $\beta/\nu = 0.11$; (b) $\nu = 0.95$ and $\beta/\nu = 0.13$. Since the critical exponents in

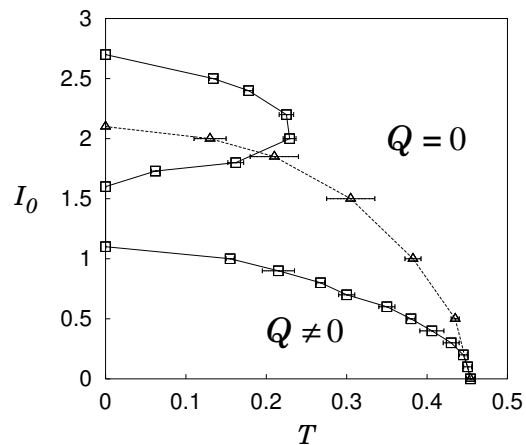


FIG. 4: Dynamic phase diagram on the $T-I_0$ plane for driving frequencies $\Omega/2\pi = 0.08(\square)$ and $0.16(\triangle)$. The boundaries are determined by the crossing points of Binder's cumulants for size $L = 8, 16$, and 24 . Again error bars have been estimated from standard deviations and lines are merely guides to eyes.

(a) agree well with those for the equilibrium Z_2 transition in the FFX Y model,^{5,10} the nice collapse of the data suggests strongly that the dynamic transition in the first ordered region [i.e., $I_0 < I_0^{(0)}$ in Fig. 2(a)] belongs to the same universality class as the equilibrium Z_2 transition of the FFX Y model. Similar conclusion was also reached in the FFJJA under weak staggered oscillating fields.⁷ On the other hand, the values in (b), corresponding to the second ordered region, appear somewhat larger than the critical exponents for the equilibrium Z_2 transition. However, due to large fluctuations, the numerical accuracy in (b) is not so good, yielding reasonable collapsing behavior down to $\nu = 0.87$ and $\beta/\nu = 0.12$. Further, note that there does exist rather large discrepancy among the equilibrium values reported in literature,^{5,10,11} which may be summed up as follows: $\beta = 0.11 \pm 0.03$ and $\nu = 0.9 \pm 0.1$. In view of this uncertainty, it is also possible to consider the values in (b) to be consistent with those for the same (equilibrium Z_2) transition. Accordingly, we presume that for all driving amplitudes the dynamic transition in the system belongs to the same universality class as the equilibrium Z_2 transition present in the FFX Y model.

IV. RESONANCE BEHAVIOR

Finally, we explore the possibility of the stochastic resonance phenomena in the FFJJA under uniform oscillating currents. In numerical simulations, we compute the power spectrum $P(\omega)$ of the staggered magnetization

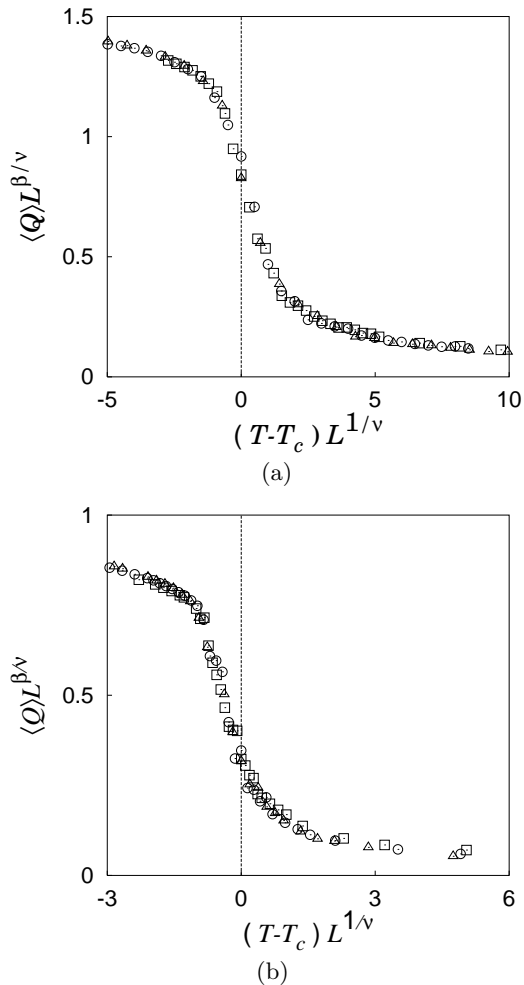


FIG. 5: Scaling plot of the dynamic order parameter versus the temperature for size $L = 16$ (\square), 24 (\circ), and 32 (\triangle) with $\Omega/2\pi = 0.08$ and (a) $I_0 = 0.3$; (b) $I_0 = 2.2$. The data fitting has been made with the equilibrium values of the critical exponents (a) $\nu = 0.82$ and $\beta/\nu = 0.11$; (b) $\nu = 0.95$ and $\beta/\nu = 0.13$.

$m(t)$ and its SNR, which is defined to be

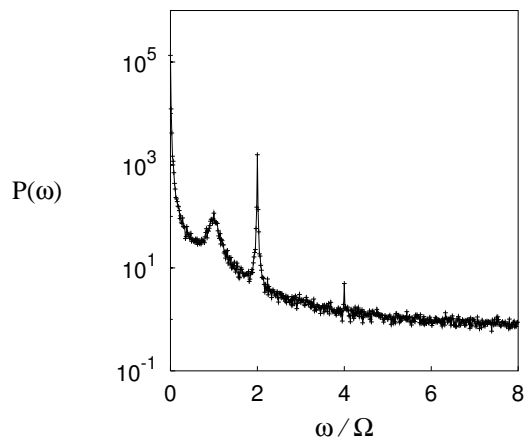
$$\text{SNR} = 10 \log_{10} \left[\frac{S}{N} \right]. \quad (8)$$

The signal S is given by the peak intensity of the power spectrum at the driving frequency Ω and N represents the background noise level, which is estimated by the average power spectrum around the signal peak. We can also define similar quantities for the higher harmonics of the driving frequency Ω , the behaviors of which are found to be quite peculiar as described below.

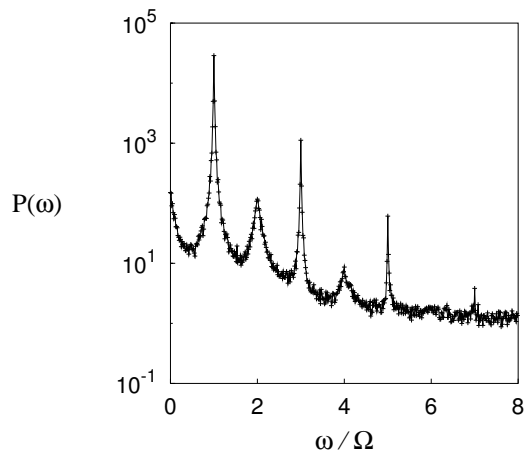
In Fig. 6, we display typical behavior of the power spectrum $P(\omega)$ at low temperatures for several driving amplitudes. Note the substantial difference according to the driving current amplitude I_0 , which may be understood in view of zero-temperature states. For $I_0 = 0.8$,

where there is no oscillation of the staggered magnetization $m(t)$ at zero temperature, observed at low temperatures are broad peaks around odd harmonics as well as sharp peaks at even harmonics, as shown in Fig. 6(a). On the other hand, for higher values of I_0 , corresponding to $Q = 0$ at zero temperature, addition of thermal noise gradually suppresses the sharp peaks at odd harmonics while inducing broad peaks at even harmonics [see Fig. 6(b)]. When the system enters another ordered region of $0 < Q < 1$ by further increase of I_0 , the staggered magnetization exhibits only oscillations of even harmonics at zero temperature, which remain as sharp peaks at finite temperatures. Here, noise again helps to develop broad peaks around odd harmonics and interestingly, the third harmonics are dominant over the first harmonics [see Fig. 6(c)].

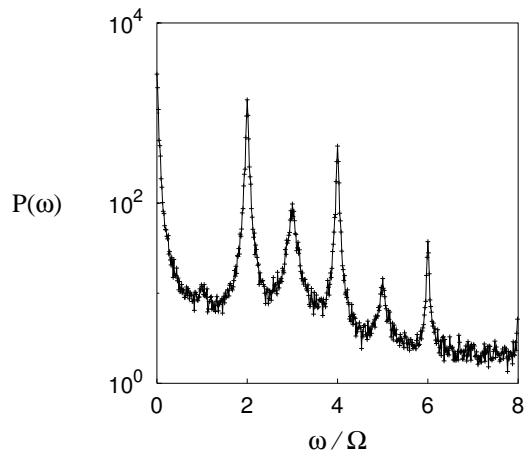
Such interesting behavior depending on the driving current amplitude is expected to bring about rich physics in the SR phenomena. The SNR computed at the first and second harmonics for $I_0 = 0.8$ is plotted in Fig. 7 (a) and (b), respectively. It is demonstrated that both the broad peak at the first harmonics and the sharp one at the second harmonics, which shows up in the presence of the noise, exhibit the SR behavior. Remarkably, the resonance temperature for the first harmonics is found to be different from that for the second harmonics: The former is higher and the dynamic transition temperature is located between the two resonance temperatures. For $I_0 = 1.2$, the SR behavior of the second harmonics is again observed as shown in Fig. 8(b). However, the SNR of the first harmonics decreases monotonically with the temperature [see Fig. 8(a)], indicating that the oscillations of the odd harmonics present in the zero-temperature state are simply suppressed by the noise. Similar argument explains the SR behaviors for $I_0 = 2.0$, where only the even harmonics exist in the oscillations of the staggered magnetization at zero temperature. The thermal noise tends to reduce the oscillations of the second harmonics, which is manifested by the monotonic decrease of the SNR in Fig. 9(a). In contrast, the SNR of the third harmonics is initially enhanced by the weak thermal noise as shown in Fig. 9(b). These interesting behaviors may be understood as follows: The thermal noise, which is not strong enough to destroy the chirality lattice, is expected to help the chirality lattice move over one more lattice barrier if the threshold is not so large. Accordingly, for $I_0 = 1.2$ corresponding to $Q = 0$ at zero temperature, the even harmonics which are absent in the ground state are induced by the thermal noise while the odd harmonics are generally suppressed. Via the same argument, one can expect that for $I_0 = 2.0$ in the second ordered region, the odd harmonics exhibit the SR behavior with the even harmonics decreasing monotonically. At higher values of I_0 , similar SR behavior is expected for odd and even harmonics according to the zero-temperature oscillations of the staggered magnetization.



(a)

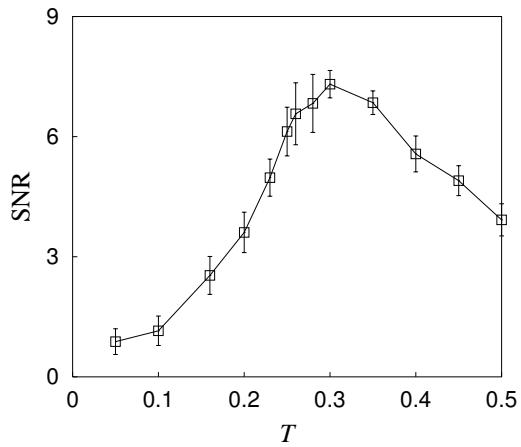


(b)

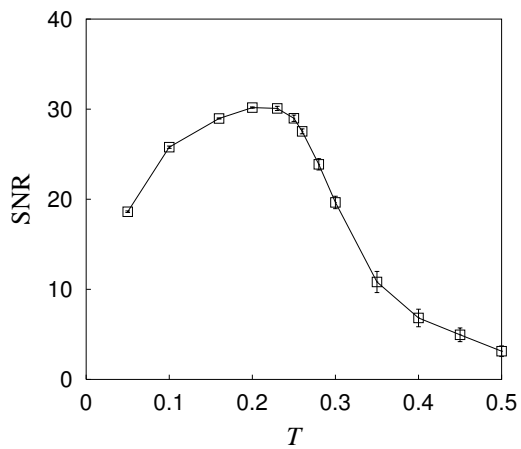


(c)

FIG. 6: Power spectrum of the staggered magnetization for size $L = 16$ and driving frequency $\Omega/2\pi = 0.08$. The driving amplitude and the temperature are (a) $I_0 = 0.8$ and $T = 0.28$; (b) $I_0 = 1.2$ and $T = 0.2$; (c) $I_0 = 2.0$ and $T = 0.3$.



(a)



(b)

FIG. 7: Signal-to-noise ratio versus the temperature in the system of size $L = 16$ with $\Omega/2\pi = 0.08$ and $I_0 = 0.8$. The signal-to-noise ratio is calculated (a) at the first harmonics and (b) at the second harmonics. Error bars have been estimated from standard deviations; lines are guides to eyes.

V. CONCLUSION

We have examined the dynamic properties of the 2D FFJJA driven uniformly by alternating currents, with attention paid to the dynamic transition and the SR phenomena. At low temperatures the chirality in the FFJJA displays antiferromagnetic ordering. To describe the dynamic transition associated with the antiferromagnetic ordering of the chirality, we have introduced the dynamic order parameter, which is the staggered magnetization averaged over one period of the oscillating current, and investigated its behavior with respect to the amplitude and the frequency of the driving current as well as to the temperature. At zero temperature, as the driving amplitude is raised, the dynamically ordered phase and the disordered one have been observed to appear alternatively. The saturation value of the dynamic order pa-

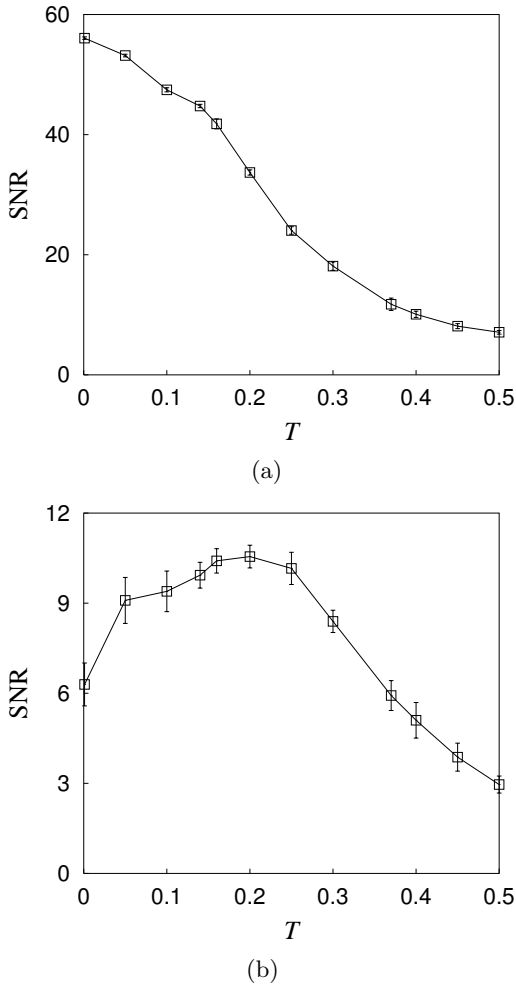


FIG. 8: Signal-to-noise ratio versus the temperature in the system of size $L = 16$ with $\Omega/2\pi = 0.08$ and $I_0 = 1.2$. The signal-to-noise ratio is calculated (a) at the first harmonics and (b) at the second harmonics. The leftmost data correspond to the temperature $T = 0.001$.

parameter is unity in the first ordered region while it is less than unity in other ordered regions. It has also been observed that the increase of the driving frequency tends to shift the dynamically ordered regions toward larger values of the driving amplitude. Except for the scale, the overall behavior at zero temperature does not change qualitatively with the driving frequency. As the temperature is increased, the ordered phase undergoes a dynamic phase transition to the disordered phase. We have obtained the phase diagram of the dynamic transition on the plane of the temperature and the driving amplitude. Through the use of the finite-size scaling analysis, the dynamic transition has been shown to belong to the same universality class as the equilibrium Z_2 transition in the FFX Y model. We have also examined the SR phenomena in the system. To investigate the phenomena, we have calculated the power spectrum of the

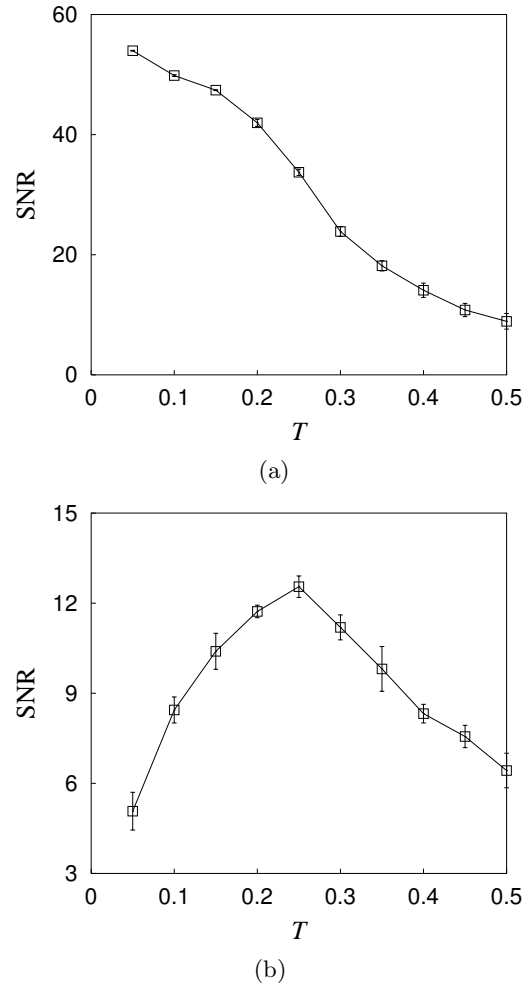


FIG. 9: Signal-to-noise ratio versus the temperature in the system of size $L = 16$ with $\Omega/2\pi = 0.08$ and $I_0 = 2.0$. The signal-to-noise ratio is calculated (a) at the second harmonics and (b) at the third harmonics.

staggered magnetization, which shows characteristic behavior according to the state at zero temperature. In the regions corresponding to finite values of the dynamic order parameter at zero temperature, broad peaks have been observed around odd harmonics as well as sharp peaks at even harmonics. On the other hand, in the regions with vanishing dynamic order parameters at zero temperature, the opposite situation has been observed. As manifested by the SNR at several harmonics, the odd and the even harmonics have been revealed to exhibit different SR behaviors, which may be understood in view of the variation of the zero-temperature states with the driving amplitude.

Acknowledgments

MYC thanks the Korea Institute for Advanced Study for hospitality during his visit, where part of this work was accomplished. This work was supported in part by

the Ministry of Education through the BK21 Program and in part by the Korea Science and Engineering Foundation through the Center for Strongly Correlated Materials Research (GSJ).

-
- ¹ T. Tomé and M.J. de Oliveira, Phys. Rev. A **41**, 4251 (1990); M. Acharyya, Phys. Rev. E **59**, 218 (1999).
² G. Korniss, C.J. White, P.A. Rikvold, and M.A. Novotny, Phys. Rev. E **63**, 016120 (2000).
³ K.-T. Leung and Z. Nédá, Phys. Rev. E **59**, 2730 (1999); B.J. Kim, P. Minnhagen, H.J. Kim, M.Y. Choi, and G.S. Jeon, Europhys. Lett. **56**, 333 (2001).
⁴ K.K. Mon and S. Teitel, Phys. Rev. Lett. **62**, 673 (1989); J.S. Chung, K.H. Lee, and D. Stroud, Phys. Rev. B **40**, 6570 (1989); S. Kim and M.Y. Choi, *ibid.* **48**, 322 (1993).
⁵ H.J. Luo, L. Schülke, and B. Zheng, Phys. Rev. Lett. **81**, 180 (1998).
⁶ V.I. Marconi and D. Domínguez, Phys. Rev. Lett. **87**, 017004 (2001).
⁷ G.S. Jeon, H.J. Kim, M.Y. Choi, B.J. Kim, and P. Minnhagen, Phys. Rev. B **65**, 184510 (2002).
⁸ B.J. Kim, P. Minnhagen, and P. Olsson, Phys. Rev. B **59**, 11506 (1999).
⁹ K. Binder, Phys. Rev. Lett. **47**, 693 (1981).
¹⁰ S. Lee and K.-C. Lee, Phys. Rev. B **49**, 15184 (1994).
¹¹ E. Granato and M.P. Nightingale, Phys. Rev. B **48**, 7438 (1993); P. Olsson, Phys. Rev. Lett. **75**, 2758 (1995); J.V. José and G. Ramírez-Santiago, *ibid.* **77**, 4849 (1996).